International Conference on Space Optics—ICSO 2018

Chania, Greece

9–12 October 2018

Edited by Zoran Sodnik, Nikos Karafolas, and Bruno Cugny

Modular and smooth introduction of photonics in high-throughput communication satellites – perspective of project BEACON

Vanessa Duarte

João Prata

Rogério Nogueira

Georg Winzer

et al.

esa icso proceedings cnes

International Conference on Space Optics — ICSO 2018, edited by Zoran Sodnik, Nikos Karafolas, Bruno Cugny, Proc. of SPIE Vol. 11180, 1118079 · © 2018 ESA and CNES · CCC code: 0277-786X/18/$18 · doi: 10.1117/12.2536180

Modular and smooth introduction of photonics in high-throughput communication satellites – perspective of project BEACON

Vanessa C. Duarte[a,b], João G. Prata[a], Rogério N. Nogueira[a,c], Georg Winzer[b], Lars Zimmermann[b], Rob Walker[d], Stephen Clements[d], Marta Filipowicz[e], Marek Napierała[e], Tomasz Nasiłowski[e], Jonathan Crabb[f], Leontios Stampoulidis[f], Javad Anzalchi[g] and Miguel V. Drummond[a]
[a]Instituto de Telecomunicações, 3810-193, Aveiro, Portugal; [b]IHP – Innovations for High Performance Microelectronics, 15236 Frankfurt (Oder), Germany; [c]Watgrid Lda., 3810-193, Aveiro, Portugal; [d]aXenic Ltd., Sedgefield, UK; [e]InPhoTech Sp. z o.o., Warsaw, Poland; [f]Gooch & Housego, Torquay, UK; [g]Airbus Defence & Space, Stevenage, UK.

ABSTRACT

In this paper we present a 4-channel silicon photonic true-time delay (TTD) beamformer in which the phase of each channel is automatically adjusted in real-time. Beamforming was demonstrated with a 1 Gb/s QPSK signal carried at 28 GHz. The demonstration comprised the following custom made devices: two arrays of GaAs Mach-Zehnder modulators (MZMs), a radiation-hardened 7-core erbium-doped fiber amplifier (MC-EDFA) for power boosting, and a silicon photonic integrated circuit (PIC) containing a 4×1 TTD optical beamformer network (OBFN). Having provided a successful proof-of-concept demonstration, the dimensioning of an end-to-end photonic-aided payload receiver is here studied. It comprises the proposed OBFN fed by 100 antenna elements (AEs) in a multibeam scenario, also providing an estimation of the system's power consumption.

Keywords: Radio frequency photonics; Integrated optics, Phased-array radar, Satellite communications.

1. INTRODUCTION

High-throughput communications satellites allow the access of a large number of users to wireless broadband, as a single system is able to cover entire continents with multiple spot beams [1, 2]. Communications satellites currently face two main challenges. First, the increasing bandwidth demand is pushing for an increase in number and density of beams; second, the geographic distribution of bandwidth demand changes over the lifetime of a satellite, thus requiring flexible coverage.

Large-scale photonic-aided payloads are a promising approach to provide high-capacity and yet flexible coverage. Photonic-aided payloads build on basic microwave photonics devices such as tunable filters [3] or tunable optical delay lines (TODLs) [4, 5], which are part of a photonic processor referred to OBFN [6]. Since the replacement of RF by photonic components in common payloads has not been fully addressed, a complete dimensioning of photonic-aided payloads is a key gap needed to be filled and discussed in detail.

In this paper, we provide a first experimental demonstration of an OBFN [6] that mimics an RF beamformer. The demonstration comprises two arrays of GaAs MZMs for modulation, a radiation-hardened optical amplifier based on a 7-core MC-EDFA for power boosting, and a silicon PIC containing a 4x1 TTD OBFN. The time delay and phase of each of the four input signals are automatically adjusted in real-time, thus providing robust operation. Four copies of a 1 Gb/s QPSK signal with a 28 GHz carrier were used as K_a-band test signals. Beamforming was achieved by observing a fourfold increase in output amplitude and a reduction of the error vector magnitude (EVM) of the same order. An end-to-end system dimensioning is also done, in which starts with a simple estimation of the power consumed by each stage of the system, followed by the dimension the complete system as a function of the signal to noise ratio (SNR), power consumption and beam crosstalk.

2. EXPERIMENTAL SETUP & RESULTS

The experimental setup is shown in Figure **1** (a). A laser signal with a linewidth of 100 kHz and a wavelength of 1550.1 nm is split in three paths. Modulation of input RF signals is performed in the two upper paths, whereas a frequency-

shifted optical local oscillator (FSOLO) is generated in the lower path. An arbitrary wave generator (AWG) is used to generate a 1 Gbit/s QPSK signal with 640 symbols, 28 GHz carrier, raised-cosine pulse shaped with a roll-off factor of 0.25, and with two pilot tones at 28 ± 0.6 GHz. Four copies of such RF signal are generated, amplified and fed to two arrays of modulators [7], each with two MZMs. Each modulator array outputs two polarization-multiplexed optical signals, which are pre-amplified, noise filtered and then polarization demultiplexed. Each of the four resulting optical signals is delayed by a mechanical delay line such that signal path lengths are equalized within the tuning range of the TODLs of the OBFN. Each of the resulting signals is then boosted by a core of the MC-EDFA [8]. The output power of each amplified signal is adjusted by a variable optical attenuator (VOA) before being fed to the PIC through quasi-vertical coupling.

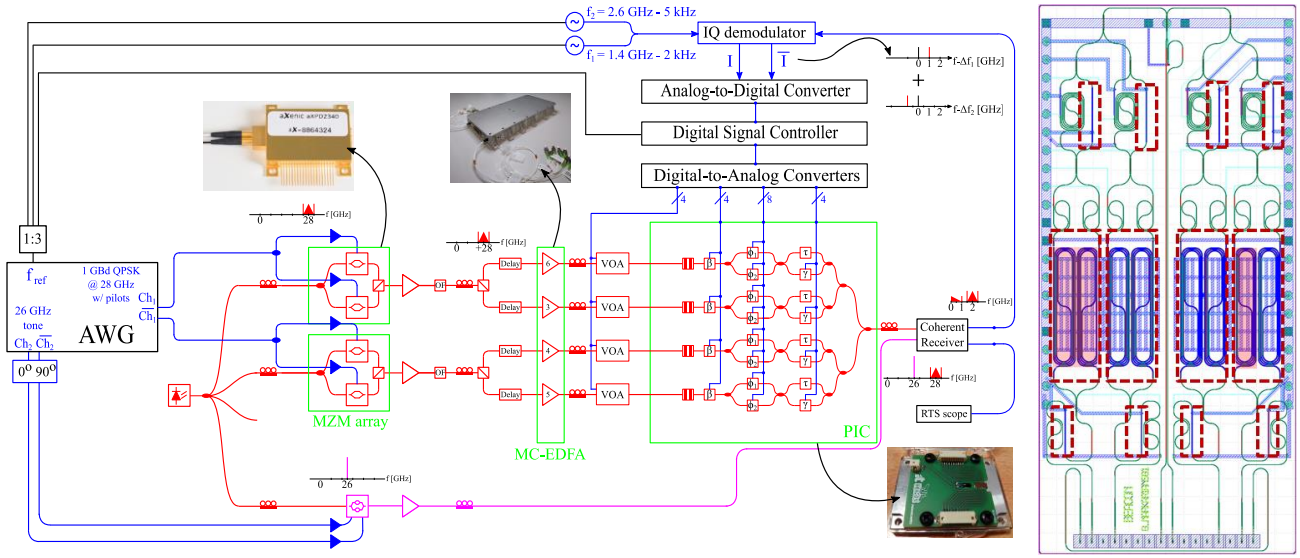

(a) (b)

Figure 1. (a) Experimental setup of the $\mathbf{4 \times 1}$ OBFN. (b) Layout of the silicon PIC.

The PIC comprises four identical paths, each with an input phase shifter for adjusting the phase of each path, a TODL based on a Mach-Zehnder delay interferometer (MZDI) with tunable coupling ratio [4, 6] and with a tuning range of $\tau = 50$ ps. The four paths are then combined into one output signals, which in turn is split in two copies. One copy is combined with an input optical signal and fed to a germanium photodiode, providing the possibility of performing coherent detection. Such possibility was not explored in this experiment. The other copy is routed to a grating coupler, such that the beamformed signal can be processed outside of the PIC.

The PIC layout is shown in Figure **1** (b), with the used phase shifter highlighted with red squares, i.e., coiled heaters are not used. Bottom to top, for each path there is an input carrier-injection phase shifter with 500 µm (β), two coiled carrier-depletion phase shifters with 1 cm ($\phi_{1,2}$) for tuning the TODL delay, and another carrier-injection phase-shifter with 500 µm (γ) for adjusting the detuning (Δf) between the center frequency of the MZDI and the processed optical signal. The reason why all three common kinds of silicon photonics phase shifters were used was to test their suitability to the proposed system, which we did and reported in [9]. The PIC was bond-wired to a printed circuit board (PCB) in order to provide access to the used phase shifters. During initial characterization, three phase shifters, identified in the figure in light red, did not respond to an applied voltage. We found out that it was due to a design error. The implication was that time delay tuning is not possible in the first (upper) path. Such is not problematic as the upper path may serve as the time reference, to which the time delays of the remaining three paths are tuned. As for the fourth path, delay tuning was achieved with the only functional carrier-depletion phase shifter.

In the lower path, the input laser signal is modulated by an IQ modulator (IQM) fed by two 26 GHz tones in quadrature, thus producing a FSOLO. The FSOLO is amplified before being fed to a single-polarization coherent receiver together with the OBFN output signal. Given that the OLO is frequency-shifted by 26 GHz, the signal produced by coherent detection is downconverted to 2 GHz.

The downconverted signal is split in two copies, one of which is input to a real-time sampling scope for offline evaluation of the signal, and the other is fed to a control loop, to calculate the voltages to be programmed to the digital-to-

analog converters, which in turn actuate on VOAs and phase shifters. The control loop starts by RF downconverting the pilot tones at 2 ± 0.6 GHz to 5 kHz and 2 kHz, respectively, in a single RF IQ demodulator. The RF downconverted pilots are then digitized at 64 ksa/s, and processed by a digital signal controller (DSC). The DSC performs fine frequency downconversion to baseband, and calculates the power and phase of each pilot tone, P_1, P_2, δ_1 and δ_2. The signal power is estimated from P_1, the detuning Δf from $P_2 - P_1$, and the delay from $\delta_2 - \delta_1$. Given that these parameters are fairly static, these are estimated and adjusted one path at a time by fully attenuating other paths except the one being analyzed. The phase of each path, however, cannot be assumed as static as it wanders over time. In order to simultaneously estimate the phase of all paths weak dithering tones with different frequencies (0.5: 0.5: 2 kHz) are digitally generated and fed to the PIC input carrier-injection phase-shifters β. Such tones are then retrieved by the DSC, which thus estimates the phase of each path and adjusts the voltage applied to the phase-shifters.

The first step in TTD beamforming is to define the delay of each path. With the proposed system, such delay can be tuned between 0 and $\tau = 50$ ps. The tuning process of the proposed TODL is shown in Figure **2**. As observed in the leftmost plots, the first path results in an estimated time delay of 0 ps, and thus is used as time reference. The remaining plots show that the TODL of the second path can be tuned within its full range. First (top plots), the detuning $\Delta f \propto P_2 - P_1$, is minimized until power difference is within ± 1 dB by adjusting V_γ (bottom plots). Then, $V_{\phi 1,2}$ are adjusted until the estimated delay is within the target delay ± 5 ps (middle plots). Results show that the achieved delay remains stable over time, thus validating the approach of tuning the delay of one path at a time. Identical results were obtained third and fourth paths, despite being useless to change $V_{\phi 1}$ in the latter.

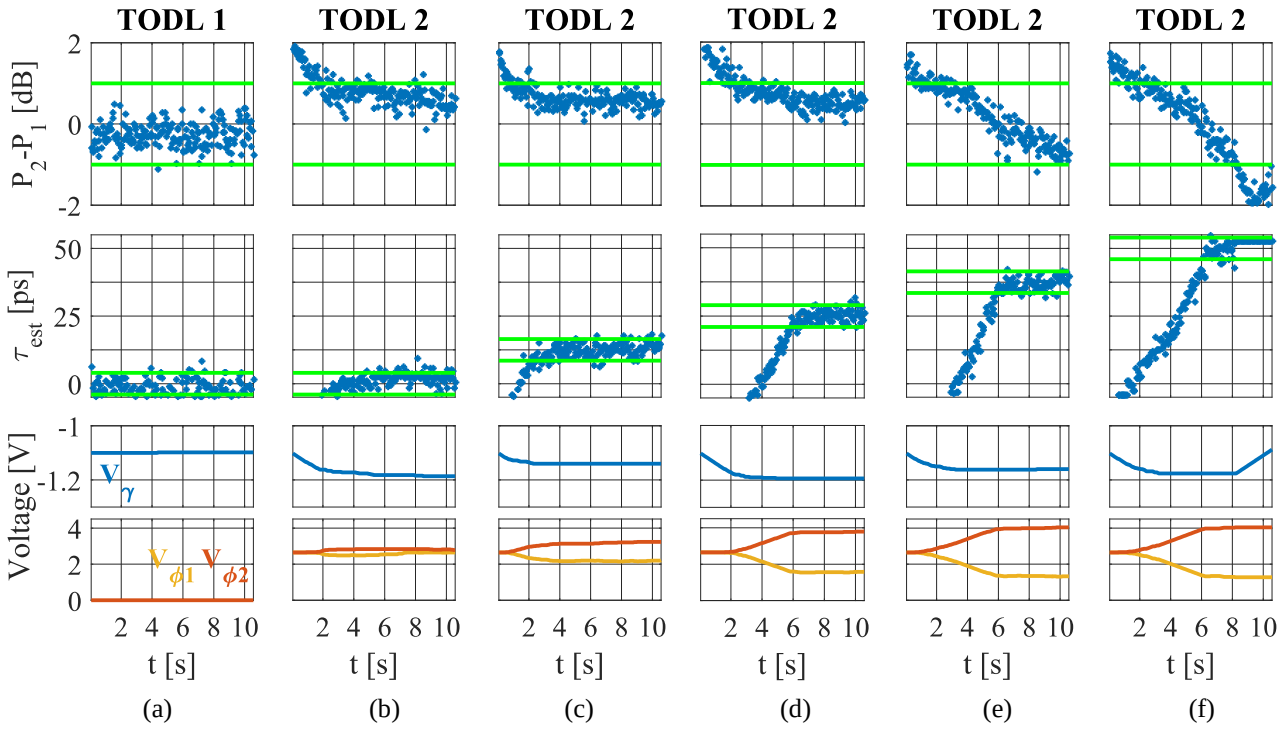

Figure 2. (a) TODL 1 serving as time reference. (b-f) Tuning of TODL 2 for different target delays. Up: Minimization of TODL. Detuning $\Delta \boldsymbol{f} \propto \boldsymbol{P_2 - P_1}$; middle: convergence of the time delay towards the target value; bottom: voltages applied to the phase shifters.

After properly setting the TODLs, real-time beamforming was performed by defining and stabilizing the phase of each path. In order to validate beamforming, all four signals were added in phase and with identical input powers, aiming to increase the output signal amplitude by a factor of four. Some obtained constellations, EVM and output signal amplitude are shown in Figure 3. The constellations show that regardless of the extra attenuation set by the VOAs, there is a clear improvement when the number of enabled paths is doubled. The expected fourfold improvement was verified in the amplitude of the downconverted QPSK signals, and also in the decrease of the EVM for an extra attenuation of 12 dB, given that for such attenuation the EVM floor of ~23% is not achieved not even for four enabled paths. Nonetheless, the

main objective of beamforming is to improve the signal-to-noise ratio of the output signal, which means that a signal beamformed from N paths and with an extra attenuation (measured in the electrical domain) of $4N$ should have an EVM lower than a signal beamformed from $N/2$ paths and with an extra attenuation of N. As indicated by the black dashed lines, such was also verified in three out of the four cases

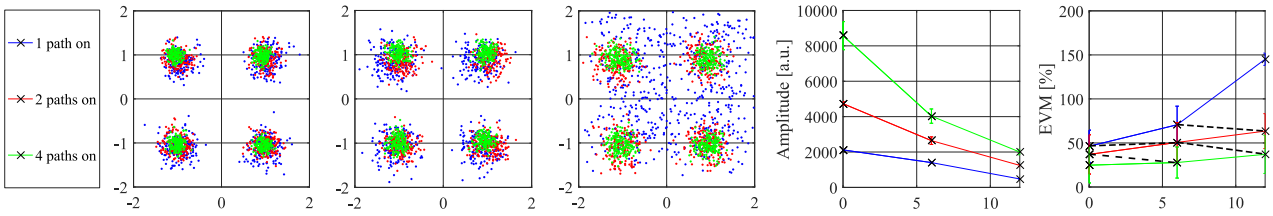

(a) Extra Att. = 0 dB (b) Extra Att. = 6 dB (c) Extra Att. = 12 dB (d) Extra Att. [dB] (e) Extra Att. [dB]

Figure 3. (a-c) Best constellations obtained for **1**, **2**, and **4** enabled paths for an extra attenuation of **0**, **6** and **12 dB**. (d) Average amplitude and (e) EVM of the output QPSK signals. Error bars quantify the standard deviation over **100** measured frames.

3. END-TO-END SYSTEM DIMENSIONING

Current RF payloads rely on coherent combination of signals followed by heterodyne detection such that uplink signals are frequency-downconverted into downlink beams [10]. To ensure a smooth transition to photonics, the photonic payloads have to follow the same reasoning as for RF payloads. Hence, the first proposed schemes start with a photonic version of the RF Bent Pipe, a photonic analog payload. In [10], we propose a new generation of photonic-aided payloads where all the signal processing is done in the optical domain. In Figure **4** is depicted the proposed payload. Here a phased array antenna (PAA) feeds the input RF stage. The signals are filtered by a low-pass filter and each signal is amplified by a low noise amplifier (LNA), as previously mentioned. The LNA output RF signal is converted to the optical domain by means of an electro optic modulator (EOM), such as a MZM modulated in the minimum transmission point. The optical signals are originated from a single reference laser source (RLS) and transmitted through short fiber links until the OBFN, not having the need of multiplexing stages. The OBFN can be considered as a coherent multiple-input multiple-output (MIMO) processor where each signal can be differentiated by beam and are fed to an array of balanced photodiodes (BPDs). At the same time a FSOLO, shifted by Δf,generated by the RLS, is also fed to the BPD array and the signal self-heterodyne detected. The output electrical signal is fed to the RF stage, where the high power amplifier (HPA) subsystem amplifies the signals and feeds to the PAA through the output multiplexer (OMUX), to be transmitted.

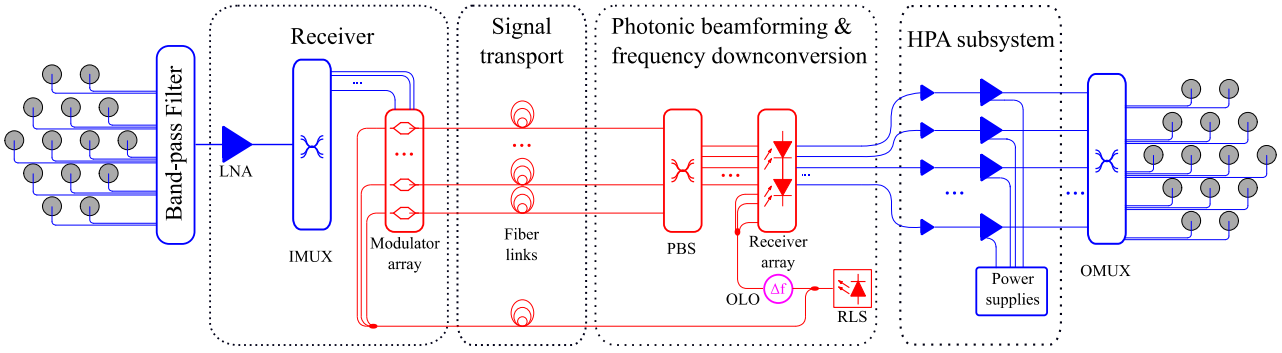

Figure 4. Simplified schematics of the proposed photonic payload transponder.

The main advantage of any photonic-aided payload is that signal transport resorts to optical fibers, which are less lossy and much lighter than coaxial cables, as referred previously. Nonetheless, there are other advantages such as the system relying to heterodyne detection makes the RF phase shifting equivalent to optical phase shifting [6].

Now, let us consider that the RF signal is in the K_a-band, $f_{RF} = 30$ GHz, and that the RLS has a wavelength of $\lambda = 1550$ nm. Since a OBFN comprises waveguides, couplers and phase shifters, and that, all of those, have a size proportional

to the operating wavelength, the OBFN can be miniaturized by a factor of $(c/\lambda)/f_{\mathrm{RF}} \approx 5000$ [10]. Such advantage confirms that the proposed system complies with a huge decrease of mass. Nevertheless, the power consumption is also of high importance.

A simple estimation of the total power consumption can be made by first considering how each active component scales with the number of input feeds, N, and the number of beams, N_{B}. Taking into account that each AE outputs two signals from each received polarization the number of LNAs is given by $2N$, optical amplifiers (OAs) is of $2N + 2N_{\mathrm{B}}$, and transimpedance amplifiers (TIAs) of N_{B}. The OBFN comprises then $N \cdot N_{\mathrm{B}}$ phase shifters, with no TTD, and the power consumption required to generate the total laser power is the power generated with a given efficiency. With $N = 1116$, a laser power 100 mW of per AE, gives a total of 112 W, with a laser generation efficiency of 25%. Regarding the power consumption of the rest of the devices, LNA, OA, TIA and phase shifter is of 1.5 W, 2 W, 0.5 W and 1 mW, respectively [10]. The power consumption of all devices is shown in Figure **5**.

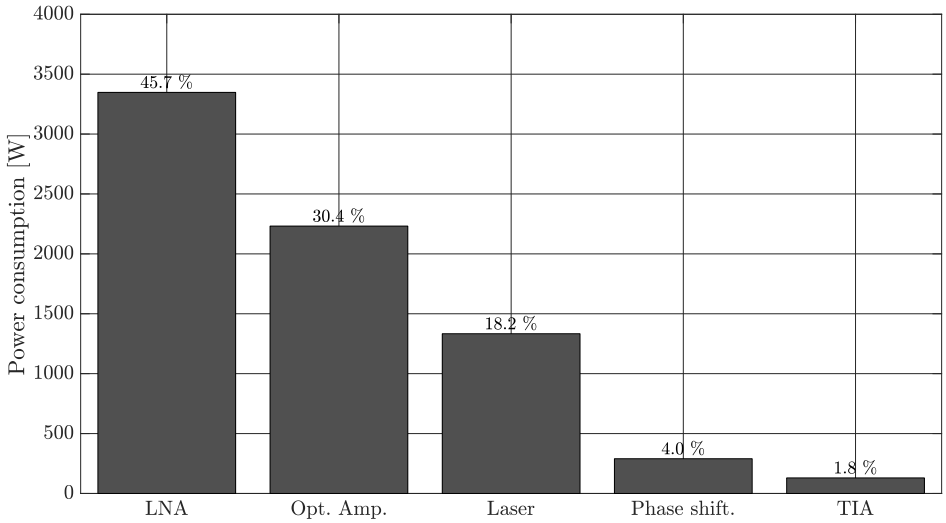

Figure 5. Power consumption of all devices considered in the proposed payload. Total power consumption is of 9.7 kW.

As observed, the majority of power consumption is consumed by the LNA and OA, totaling 76.1%. Given the low power consumption of each phase shifter of 1 mW, the OBFN only consumes 4% of the total power consumption. However, if each phase shifter consumes 10 mW, the power consumed by all phase shifters would increase to 23.5% of the total power consumption, now being on the same level as LNA.

For dimensioning the PAA and the OBFN to an end-to-end system, the main concern remains the one referred above: reducing the mass and power consumption. To achieve this target, the number of components must be also reduced. Such can be possible with the array thinning. However, array thinning also bring consequences. For instance, the SNR decreases, and due to the limited side lobe suppression in the array factor, the beam crosstalk becomes more evident. A trade-off between SNR, power consumption and beam crosstalk must be quantified.

The SNR of the output signal can be modeled then, as referred in [10], by

$$\mathrm{SNR}_{\mathrm{out}} = \frac{P_{\mathrm{out}}}{P_{n,\mathrm{AE}} + P_{n,\mathrm{OA}} + P_{n,\mathrm{out}}}$$

where P_{out} is the average output power, $P_{n,\mathrm{AE}}$ is the noise power associated with all input RF signals, i.e., antenna and feed noise, noise temperature and LNA noise attributions, $P_{n,\mathrm{OA}}$ is the noise power contribution from the OA, mainly coming from the ASE, and $P_{n,\mathrm{out}}$ as the power noise coming from the output sources, i.e., PD shot noise and TIA noise.

In the case of the beam crosstalk, a total of 50 beams with same polarization and frequency are considered within a span of $\pm 3.57 \times \pm 0.42^{\mathrm{o}}$, in which 100 realizations are run, each of which has a random selection of N AEs out of the 19927 AEs of the filled array [10].

Figures of merit are shown in Figure **6**. Since the power consumption limits the number of AE to around 100 [12], the SNR is of 20 dB with a beam crosstalk of 21 dB. Looking to the power consumption plot, a total of 896 W is consumed,

in which approximately half derives from the optical devices and the other half from the RF components. If comparing with Figure **5**, the it is observed that the OAs are consuming 12% less power than previously calculated, however this difference is replaced by the TIAs consumption.

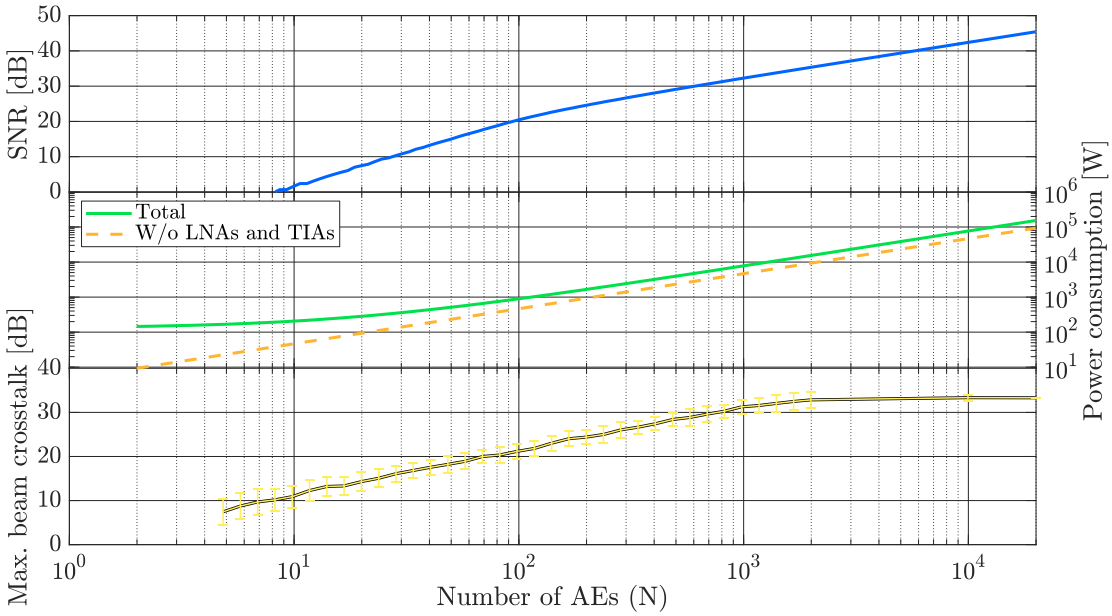

Figure 6 SNR, power consumption and beam crosstalk as a function of the number of AEs. The error bar is given by the standard deviation of the **100** realizations.

4. CONCLUSIONS

A first experimental demonstration a self-heterodyne photonic beamformer was reported, comprising two arrays of GaAs MZMs, a 7-core MC-EDFA, a silicon PIC implementing a 4×1 TTD OBFN and a real-time control system. TTD beamforming was validated using a 1 Gb/s QPSK signal with a 28 GHz carrier, resulting in a fourfold increase in output amplitude, an EVM reduction of the same order, and in an improvement of the signal-to-noise ratio.

A complete system based on the proposed concept was dimensioned, in which the SNR, power consumption and maximum beam crosstalk are calculated as a function of the number of antenna elements of the thinned phased-array antenna. We estimate that with a typical number of antenna elements of 100, an SNR and maximum beam crosstalk of about 20 dB can be reached with a power consumption below 1 kW.

FUNDING

Fundação para a Ciência e a Tecnologia (FCT) (SFRH/BD/117444/2016); European Regional Development Fund (ERDF) (FEDER) (UID/EEA/50008/2013); FP7 Space (SPACE) (FP7-SPACE-2013-1-607401).

REFERENCES

[1] Inigo, P., Vidal, O., Roy, B., Alberty, E., Metzger, N., Galinier, D, Anzalchi, J., Huggins, G. and Stirland, S., "Review of terabit/s satellite, the next generation of HTS systems," in Advanced Satellite Multimedia Systems Conference and the 13th Signal Processing for Space Communications Workshop (ASMS/SPSC) (2014), pp. 318-322.

[2] Khan, F., "Mobile internet from the heavens," arXiv:1508.02383, 2015.

[3] Capmany, J., and Novak, D., “Microwave photonics combines two worlds," Nature photonics, vol. 1, no. 6, p. 319, 2007
[4] Drummond, M. V., Monteiro, P. P., and Nogueira, R. N., “Photonic true-time delay beamforming based on polarization-domain interferometers,” J. Lightwave Technol., vol. 28, no. 17. pp. 2492–2498, Sep. 2010.
[5] Meijerink, A., et al., “Novel ring resonator-based integrated photonic beamformer for broadband phased array receive antennas—Part I: Design and performance analysis,” J. Lightwave Technol., vol. 28, no. 1. pp. 3–18, Jan. 2010.
[6] Duarte, V. C., Drummond, M. V., and Nogueira, R. N., "Photonic True-Time-Delay Beamformer for a Phased Array Antenna Receiver based on Self-Heterodyne Detection," J. Lightwave Technol., vol. 34, 5566-5575 (2016).
[7] Walker, R. G. et. al. Electro-Optic Modulators for Space Using Gallium Arsenide. SPIE International Conference on Space Optics - ICSO 2016, p. 10562, 185 (2017).
[8] Filipowicz, M. et al. Optical amplifier based on a 7-core fiber for telecommunication satellite purposes. 2017 Optical Fiber Communications Conference and Exhibition (OFC), 1-3 (2017).
[9] V. Duarte, A. Peczek, M. Drummond, R. Nogueira, G. Winzer, D. Petousi, and L. Zimmermann, SPIE International Conference on Space Optics - ICSO 2016, p. 10562 (2017).
[10] Anzalchi, J., Inigo, P., and Roy, B., "Application of photonics in next generation telecommunication satellites payloads," Proc. SPIE 10563, 1056330 (2017).
[11] Drummond, M. V., Duarte, V. C., Albuquerque, A., Nogueira, R. N., Stampoulidis, L., Winzer, G., Zimmermann, L., Clements, S., and Anzalchi, J. “Dimensioning of a multibeam coherent photonic beamformer fed by a phased array antenna," Opt. Express, vol. 26, no. 5, pp. 6158-6171, Mar (2018).
[12] Wolf, H., Schneider, M., Stirland, S., and Scouarnec, D. "Satellite multibeam antennas at airbus defence and space: State of the art and trends," European Conference on Antennas and Propagation (EuCAP, 2014), pp. 182–185.